September 1987 LRP 331/87

EFFECTS OF LOW MAGNETIC SHEAR ON IDEAL MHD MODES OF TOKAMAK PLASMA WITH ELONGATED CROSS-SECTION

T. Tsunematsu, F. Troyon, F. Yasseen,
W.A. Cooper and A. Roy

EFFECT OF LOW MAGNETIC SHEAR ON IDEAL MHD MODES OF TOKAMAK PLASMA WITH ELONGATED CROSS SECTION

T. Tsunematsu[+], F. Troyon, F. Yasseen, W.A. Cooper and A. Roy

Centre de Recherches en Physique des Plasmas
Association Euratom - Confédération Suisse
Ecole Polytechnique Fédérale de Lausanne
21, Av. des Bains, CH-1007 Lausanne/Switzerland

ABSTRACT

The ideal MHD stability of the external kink modes is studied for the equilibria with a low magnetic shear near the axis. For $q_0 < 1$, the $m = 1$ component is driven by a mode coupling. When q_0 is slightly above unity, an off-resonant $m = 1$ component appears and this becomes dominant for the small aspect ratio ($A = 1.67$). These modes are stable for the fixed boundary case when the pressure gradient is small near the axis.

[+] Permanent address: Japan Atomic Energy Research Institute,
Tokai, Naka, Ibaraki, Japan

1. INTRODUCTION

In the design of the INTOR type of a fusion reactor, it is assumed that both beta limit and energy confinement are proportional to the total plasma current. For a fixed q_s ($q_s > 2$), the elongation of the cross section helps to increase the total current, where q_s denotes the safety factor at the plasma surface or near the plasma surface for the divertor configuration. On the other hand, the H-mode discharge is a candidate of the operational regimes of a fusion reactor. The H-mode discharge has a peaked profile of the current density and a steep pressure gradient near the plasma surface after the transition from the L-mode. For a long time discharge, the current density becomes flat in the time scale of the transport. The model of the profile in the H-mode discharge was proposed by Turnbull et al./1/.
The stability of the ideal MHD modes has been analyzed for the case of the circular cross section. By keeping the profile of the current density and increasing the elongation, the safety factor becomes flatter near the magnetic axis and steeper near the plasma surface. For the profiles given in Ref. 2 and the elongated cross section, the range of the low magnetic shear becomes wide and the shear sometimes becomes negative. Due to the toroidicity and the elongation, the external kink modes may excite the lower poloidal mode number components in the low shear region. In this paper, we show the characteristics of the external kinks modes obtained by using the ERATO code for a low shear equilibrium. The effect of the aspect ratio is also studied.

2. EQUILIBRIUM PROFILES AND SHAPE OF CROSS SECTION

In the equilibrium calculation, we solve the Grad-Shafranov equation,

$$\Delta^* \psi = - \left(R^2 p'(\psi) + T T'(\psi) \right) \qquad (1)$$

by specifying the pressure derivative, $p'(\psi)$, and the average toroidal current density,

$$I'(\psi) = \frac{2\pi}{V'} \oint_0^{2\pi} d\chi \sqrt{g} \left(\vec{j} \cdot \vec{\nabla} \phi\right) \tag{2}$$

with

$$V'(\psi) = 2\pi \oint_0^{2\pi} d\chi \sqrt{g} \tag{3}$$

where $\vec{j}$ is the plasma current density, $\sqrt{g}$ is the Jacobian, and χ and ϕ are the poloidal and the toroidal angles, respectively. For a given $p'(\psi)$ and $I'(\psi)$, $TT'(\psi)$ is obtained from

$$TT' = -\left(p'(\psi) + I'(\psi)\right) \frac{V'}{2\pi} \frac{1}{\oint_0^{2\pi} d\chi \sqrt{g}/R} \,. \tag{4}$$

The integral, $\int d\chi$, is carried out on a magnetic surface. The total current is given by

$$I = \frac{1}{2\pi} \int I'(\psi) V'(\psi) \, d\psi \,. \tag{5}$$

We use the following profiles of $I'(\psi)$ and $p'(\psi)$/1/:

$$I'(\psi) = \begin{cases} \text{quadratic function} & \psi_0 < \psi < \psi_a \\ \text{cubic function} & \psi_a < \psi < \psi_b \\ 0 & \psi_b < \psi < \psi_s \end{cases} \tag{6}$$

and

$$p'(\psi) = \begin{cases} 0 & \psi_0 < \psi < \psi_c \\ \text{cubic function} & \psi_c < \psi < \psi_d \\ \text{quadratic function} & \psi_d < \psi < \psi_s \end{cases} \tag{7}$$

where ψ_0 and ψ_s are the poloidal flux at the magnetic axis and the plasma boundary, respectively. The pressure gradient, $p'(\psi)$, is adjusted such that $p'(\psi_d)$ is a maximum. The example of these profiles is shown in Fig. 1. In the following analysis, we fix the poloidal beta value, β_I, defined as

$$\beta_I = \frac{8\pi}{\mu_0 I^2} \int p \, dS \,. \tag{8}$$

The shape of a plasma surface is specified by using the expressions,

$$r = R + a\cos(\theta + \delta\sin\theta) \qquad (9)$$

and

$$z = Ea\sin\theta \quad . \qquad (10)$$

The shape of the cross secion is determined by the major radius, R, the minor radius, a, the elongation, E, and the triangularity, δ. The aspect ratio is defined by A = R/a.

3. STABILITY DIAGRAM AND MODE STRUCTURES

We study the stability of the n = 1 external kink modes in the q_0-q_s space for a given β_I. This stability diagram gives an operational range of a tokamak plasma. In this paper, we choose two kinds of equilibria: (1) A = 3.7, E = 2.0, δ = 0.4 and β_I = 0.95 and (2) A = 1.67, E = 1.68, δ = 0.3 and β_I = 0.35. The first equilibrium is similar to a version of NET design /2/. The elongation increases the normalized current, $I_N = I_p\mu_0/aB_0$, for a fixed q_s and the beta limit is expected to increase due to the scaling law, $\beta = g\, I_N$. The second equilibrium is similar to the "natural shape" of the low aspect ratio plasma /3/. The details in the operational diagram will appear elswhere /4/.

Figure 2 shows the stability diagram in the q_0-q_s space for the case 1. As β_I increases the stable region shifts to larger q_s region /4/. The flow vectors projected to a poloidal plane are shown in Figs. 3(a), 3(b) and 3(c) corresponding to the points marked by a, b and c in Fig. 2, respectively. In Fig. 3(a), the dominant component is m = 1, where m is the poloidal mode number. As q_0 increases above 1, the m = 1 component decreases and the resonant components with m > 1 become larger (Fig. 3(b) for q_0 = 1.05 and Fig. 3(c) for q_0 = 1.15). Figure 4 shows the Fourier components of the radial displacement, $X(\sqrt{\psi}) = \sqrt{\psi}\xi\psi$. Figures 4(a), 4(b) and 4(c) correspond to the cases

marked in Fig. 2. In Fig. 4(a), the dominant component is m = 1. The derivative of X, V = , approximately gives the poloidal displacement and there appears a large poloidal flow near q = 1 surface in Fig. 3(a). This is a typical mode structure of the internal kink mode. However, this equilibrium is stable for the fixed boundary case. As we have no pressure gradient within q = 1 surface for this equilibrium, the internal kink mode is stable but the same mode structure is driven by the coupling with the other components. Even if the m = 4 component is smaller than the m = 1 component, a large flow is excited inside a plasma through the mode coupling. Figure 4(b) shows the off-resonant m = 1 component. The radial structure of the m = 1 component has no sharp derivative and the m = 1 component of the flow appears smaller than other resonant components. For $q_0 > 1.1$, the dominant component is m = 4, which is a typical structure of the external kink modes. In Figs. 5(a), 5(b) and 5(c), the average potential energy, $\langle \delta W \rangle = \int \delta W d\chi$, is shown as the function of $\sqrt{\psi}$. For $q_0 < 1$, the stability is determined by the m = 1 component through the mode coupling. When q_0 is slightly above 1, the negative contribution is given by the mixture of the m = 1 and m = 2 components. For more detailed analysis, the Fourier decomposition of δW is necessary. For $q_0 > 1.1$, the resonant behavior due to the q = 2, 3 and 4 surfaces appears in δW. However, the dominant contribution is m = 2 due to the low shear.

Figure 6 shows the stability diagram for the case 2. There appears unstable region around $q_0 = 1.05$. The region marked by I is close to the marginal state for the growth rate, $\gamma^2 \sim 10^{-5}\omega_A^2$, where $\omega_A = T_0/\sqrt{\mu_0 \rho_0} R^2$, and ρ_0 is the mass density at the magnetic axis. The flows are shown in Figs 7(a), 7(b) and 7(c) corresponding to the points a, b, and c in Fig. 6, respectively. Figures 7(a) for $q_0 = 0.9$ and 7(c) for $q_0 = 1.33$ show the similar flows to those of the case 1. However, a large m = 1 motion appears in the wide region within q = 1 surface for $q_0 \sim 1.05$. This mode is stable for the fixed boundary case.The large off-resonant motion is driven by the toroidicity and the low shear. The Fourier components of X are shown in Figs. 8(a), 8(b) and 8(c) corresponding to the points a, b and c, respectively. In Fig. 8(b), the m = 1 component is dominant. The m = 1 contribution to δW is also dominant (Fig. 9(b), and there is no resonant behavior by q = 2 surface as is in Fig. 5(b).

4. SUMMARY AND CONCLUSION

We have studied the stability of the external kink modes for the equilibria with a wide low shear region. We have shown the driven m = 1 component for the cases of $q_0 < 1$ and $1 < q_0 < 1.1$. For $q_0 < 1$ the mode structure is similar to that of the internal kink mode. However, the fixed boundary mode is stable in our case. Even when there is no pressure gradient in the low shear region, the m = 1 motion can be excited by the free boundary modes. This motion causes the reconnection of the magnetic field lines due to the resistivity and a large portion of the stored energy may be emitted. For $1 < q_0$ 1.1, a large shift of the magnetic axis may be observed for a small aspect ratio tokamak. These instabilities with the dominant m = 1 motion are excited by the low shear and the deformation of the magnetic surfaces through the toroidicity and the elongation. For the detailed analysis on the effect of the shape, the Fourier decomposition of δW is necessary.

ACKNOWLEDGEMENTS

One of the authors (T.T.) thanks Prof. F. Troyon and CRPP for the opportunity to stay in Lausanne. This work is supported in part by the Fonds National Suisse de la Recherche Scientifique.

REFERENCES

/1/ A.D. Turnbull, M.A. Secrétan, F. Troyon, S. Semenzato, R.Gruber, J. Comput. Phys. 66 (1986) 391.

/2/ The NET Team, NET Status Report, NET-Report 51 (Dec. 1985).

/3/ Y.-K. M. Peng, D.J. Strickler, Nucl. Fusion 26 (1986) 769.

/4/ F. Yasseen, W.A. Cooper, A.D. Turnbull, F.Troyon, A. Roy to be submitted to Nucl. Fusion.

FIGURE CAPTIONS

Fig. 1 The average plasma current density, the safety factor and pressure profiles with $(\psi_a-\psi_0)/(\psi_s-\psi_0)$ = 0.6 and $(\psi_b-\psi_0)/(\psi_s-\psi_0)$ = 0.8 at β_I = 0.7 for E = 2, A = 3.7 and δ = 0.4. The equilibrium is characterized by a normalized current, $I_N = I_p\mu_0/RB_0$, where B_0 is the vacuum magnetic field at the center of the chamber.

Fig. 2 The stability diagram of the n = 1 external kink mode at β_I = 0.95 for A = 3.7, E = 2 and δ = 0.4. The symbols S and U denote the stable and unstable regions, respectively. At the points a, b and c, the flow of the plasma motion projected on a poloidal plane is shown in Fig. 3.

Fig. 3 The flow patterns for (a) q_0 = 0.90, q_s = 3.71 (b) q_0 = 1.05, q_s = 2.85 and (c) q_0 = 1.15, q_s = 3.47. The dominant motion is m = 1 for the case (a). The m = 1 motion appears for the case (b) through the mode coupling. For the case (c), the flow pattern shows the kink instability of a toroidal plasma.

Fig. 4 The Fourier components of the radial displacement X for the cases (a), (b) and (c) in Fig. 2 and Fig. 3. For q_0 = 0.90 (case (a)), the dominant component is m = 1. The mode structure is similar to that of the internal kink mode. For q_0 = 1.05 (case (b)), the off-resonant m = 1 component appears through the coupling with the m = 2 and 3 components. The m = 1 component has the opposite sign to the m = 2 and 3 components. For q_0 = 1.15, the m = 1 component becomes smaller and the resonant m = 2, 3 and 4 components become dominant.

Fig. 5 The integrated potential energy on a magnetic surface, $\langle\delta W\rangle = \int_0 2\pi\delta W d\chi$, vs. $s = \sqrt{\psi}$.

Fig. 6 The stability diagram of the n = 1 external kink mode at $\beta_I = 0.35$ for A = 1.67, E = 1.68 and $\delta = 0.3$. At the points a, b and c, the flow of the plasma motion is shown in Fig. 7.

Fig. 7 The flow patterns for (a) $q_0 = 0.92$, $q_s = 3.10$ (b) $q_0 = 1.04$, $q_s = 3.74$ and (c) $q_0 = 1.33$, $q_s = 3.86$. For the case (b), a large and wide m = 1 motion appears.

Fig. 8 The Fourier components of the radial displacement X for the cases (a), (b) and (c) in Fig. 6 and Fig. 7.

fig. 9 The integrated potential energy on a magnetic surface vs. $s = \sqrt{\psi}$. For the case (b), the dominant contribution is the m = 1 component.

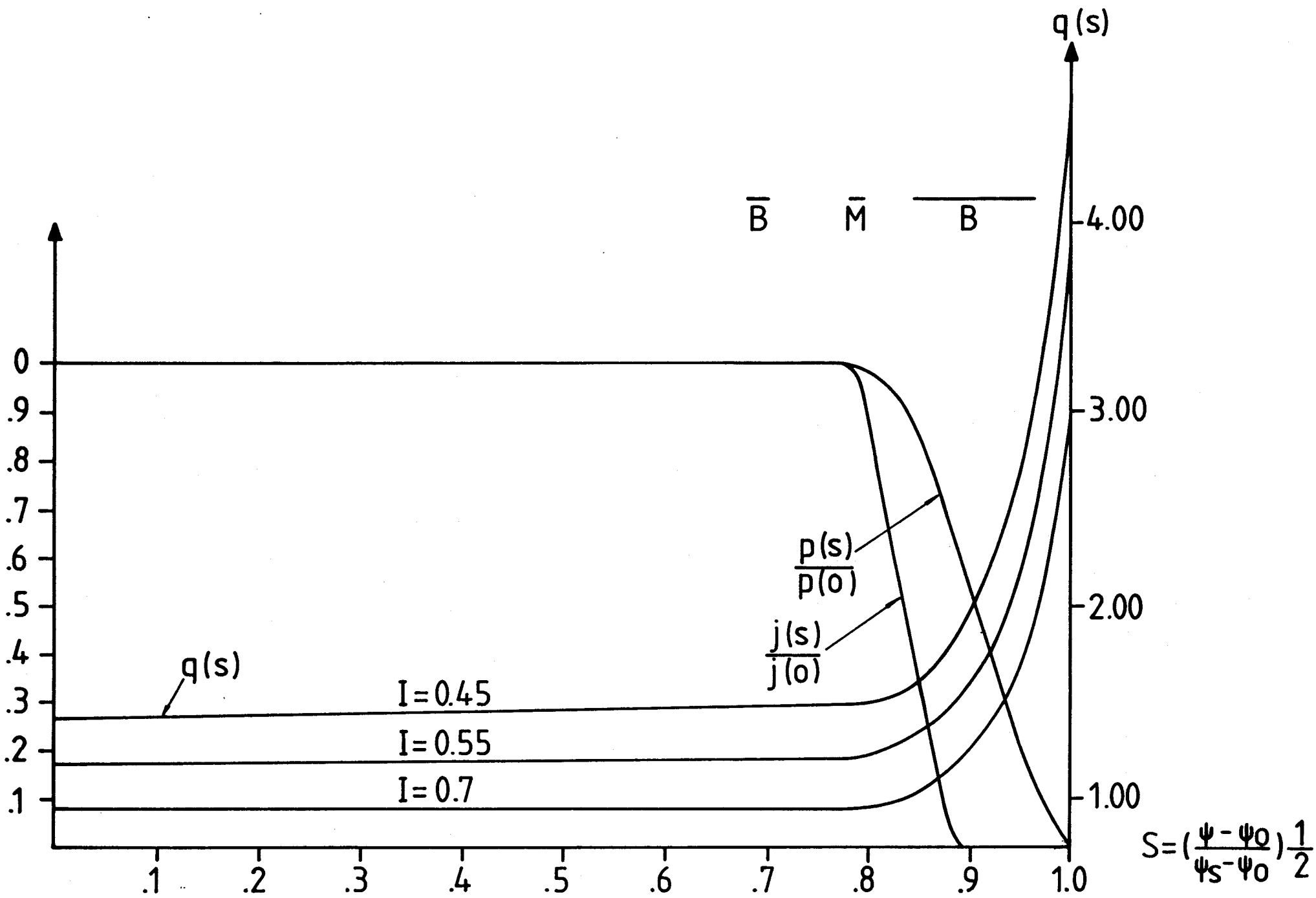
q(s)
B̄ M̄ B̄
4.00
3.00
2.00
1.00
0
.9
.8
.7
.6
.5
.4
.3
.2
.1
p(s)/p(0)
j(s)/j(0)
q(s)
I=0.45
I=0.55
I=0.7
.1 .2 .3 .4 .5 .6 .7 .8 .9 1.0
S=((ψ-ψo)/(ψs-ψo))^1/2

- Fig. 1

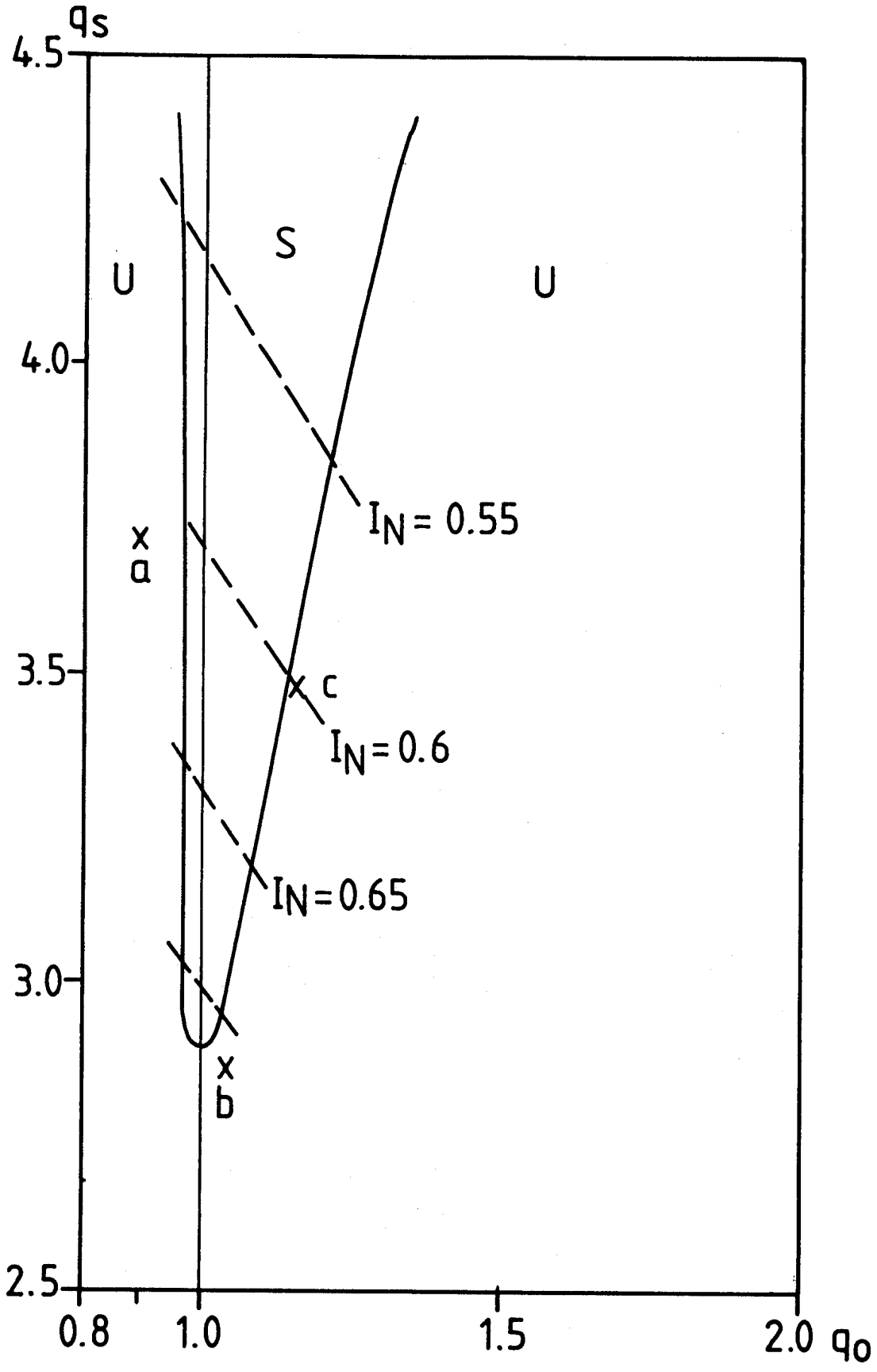

FIG. 2

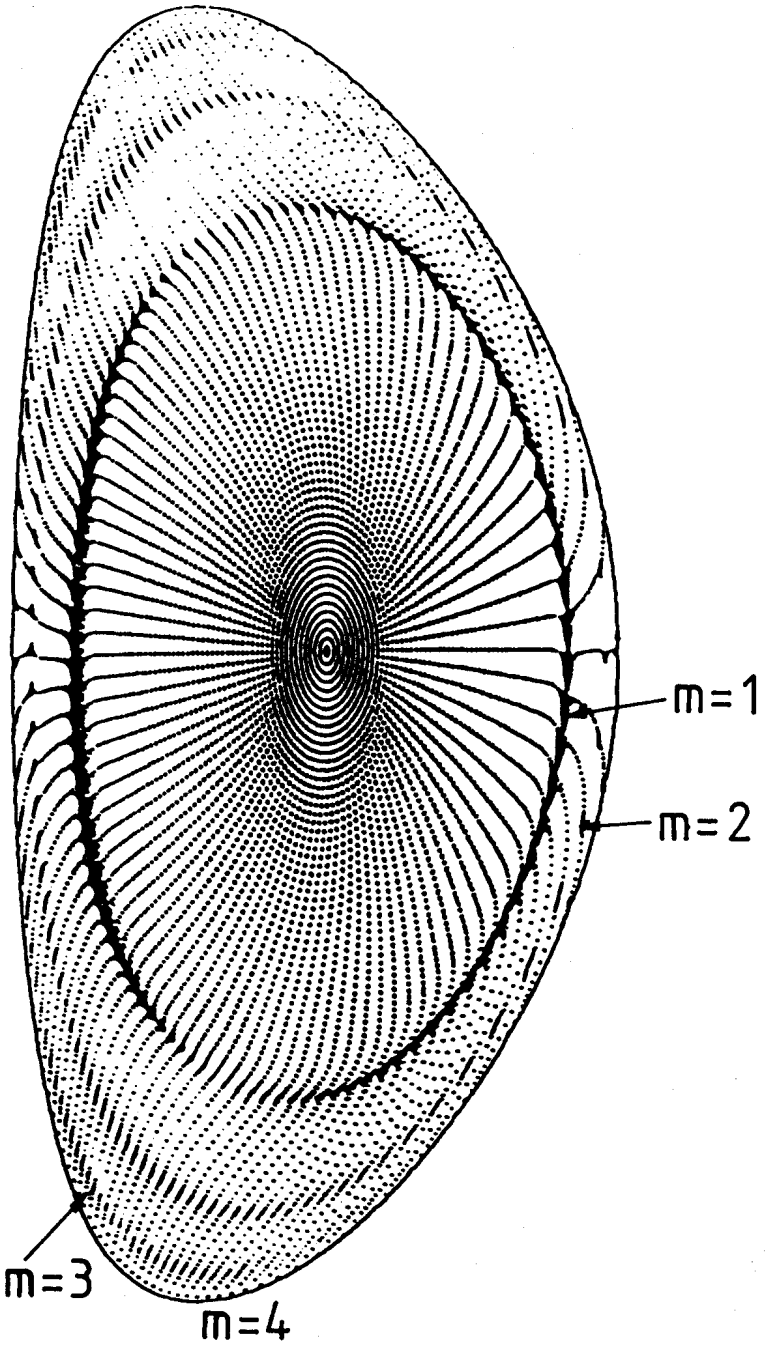

FIG. 3A

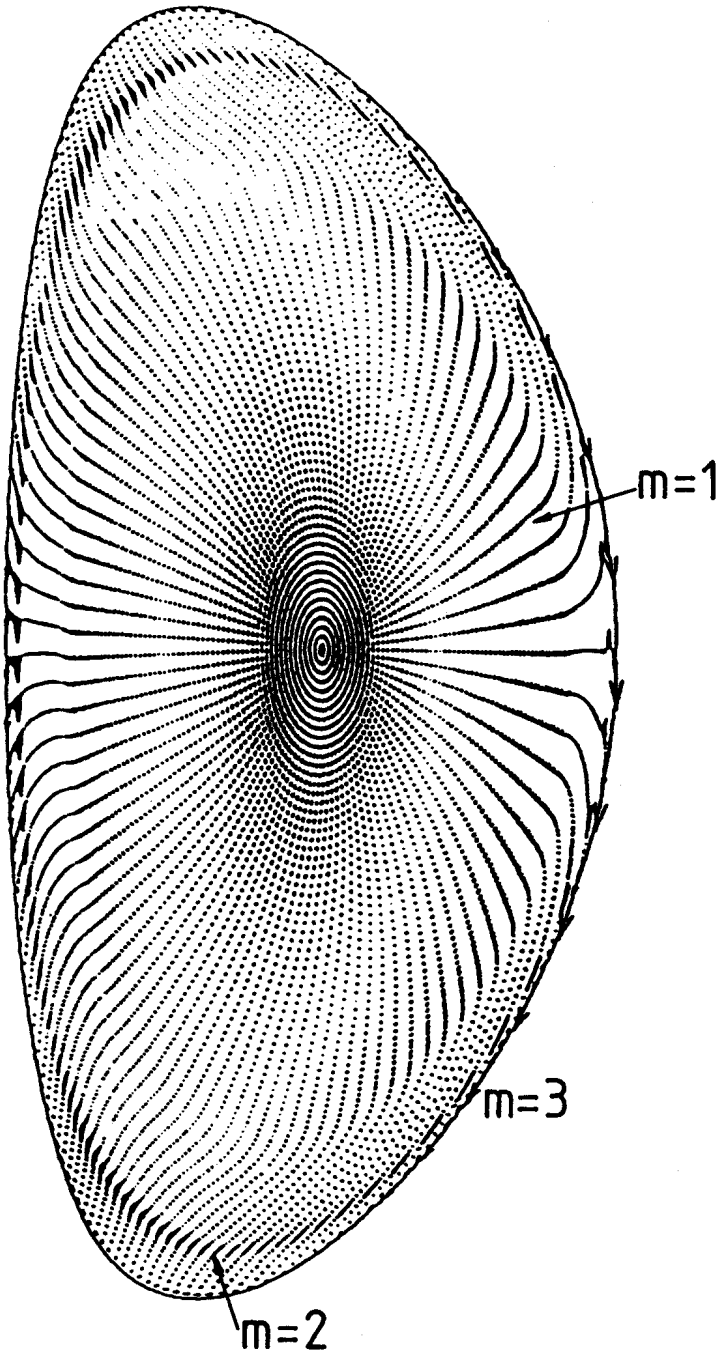

FIG. 3B

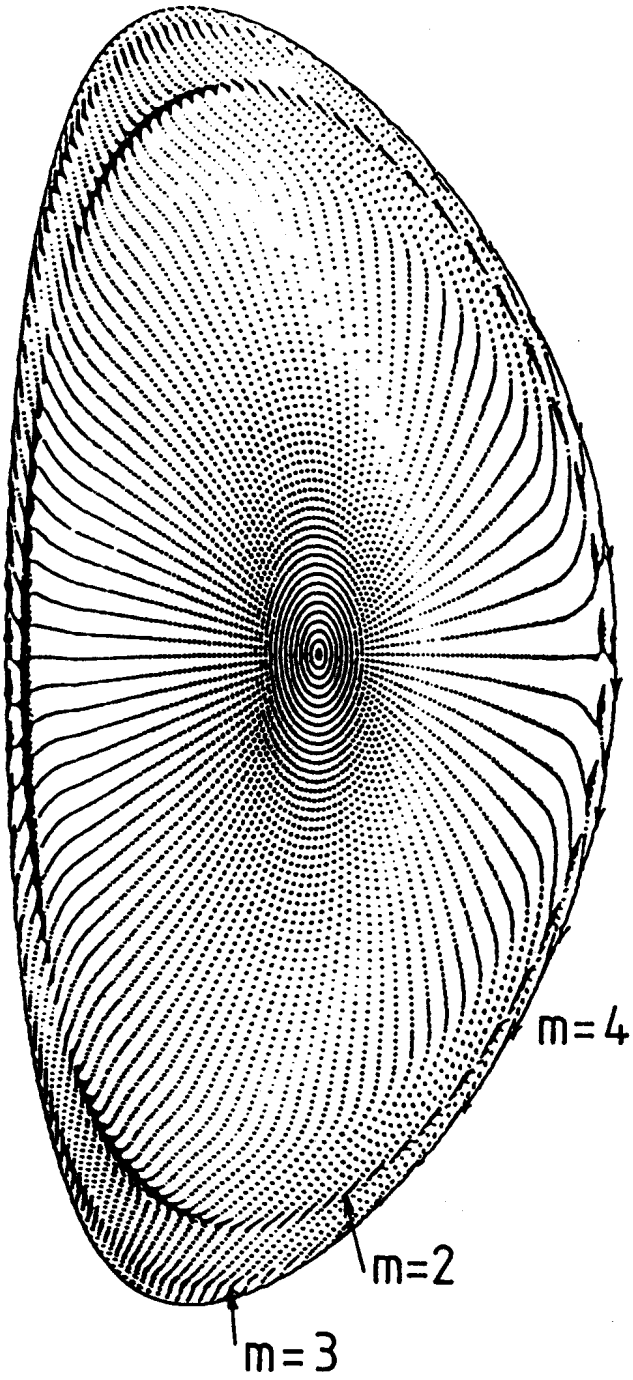

FIG. 3c

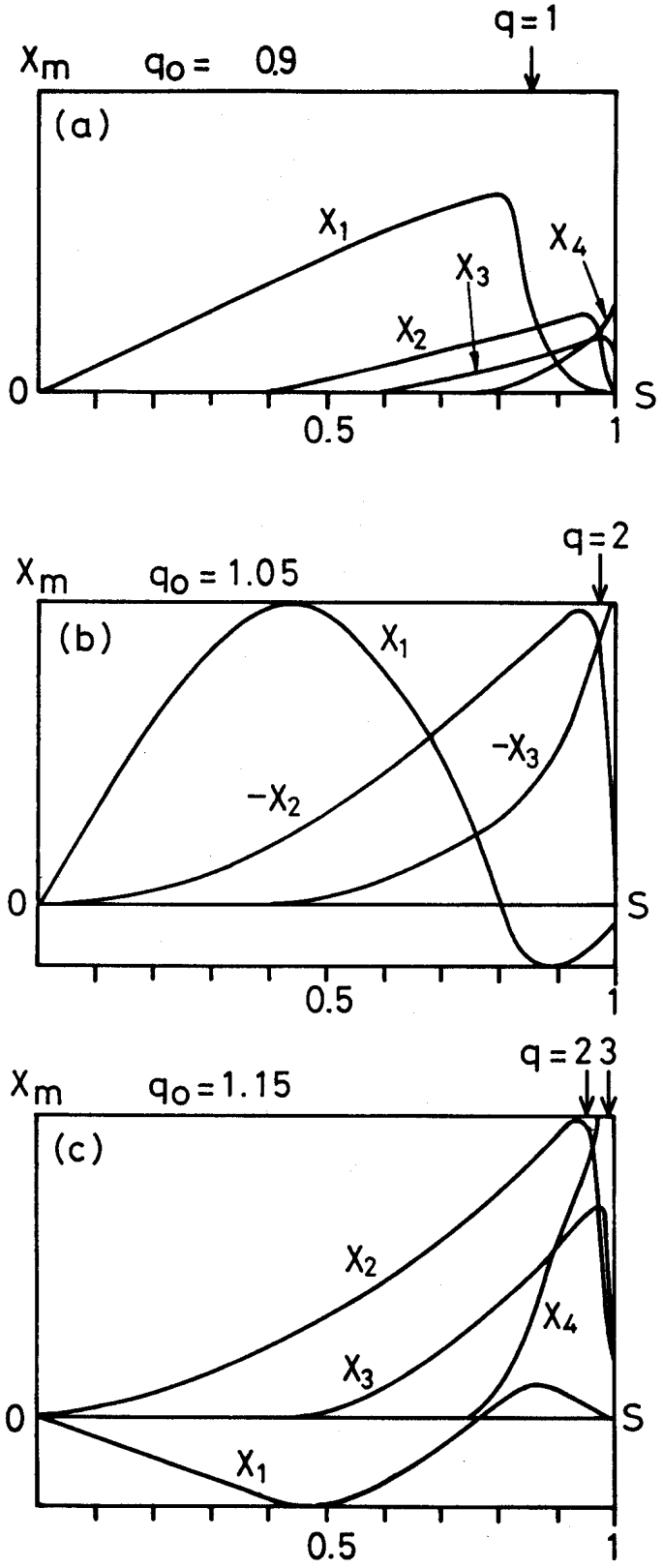
q=1
Xm
qo= 0.9
(a)
X1
X4
X3
X2
0
S
0.5
1
q=2
Xm
qo = 1.05
(b)
X1
-X3
-X2
0
S
0.5
1
q=23
Xm
qo=1.15
(c)
X2
X4
X3
0
S
X1
0.5
1

FIG. 4

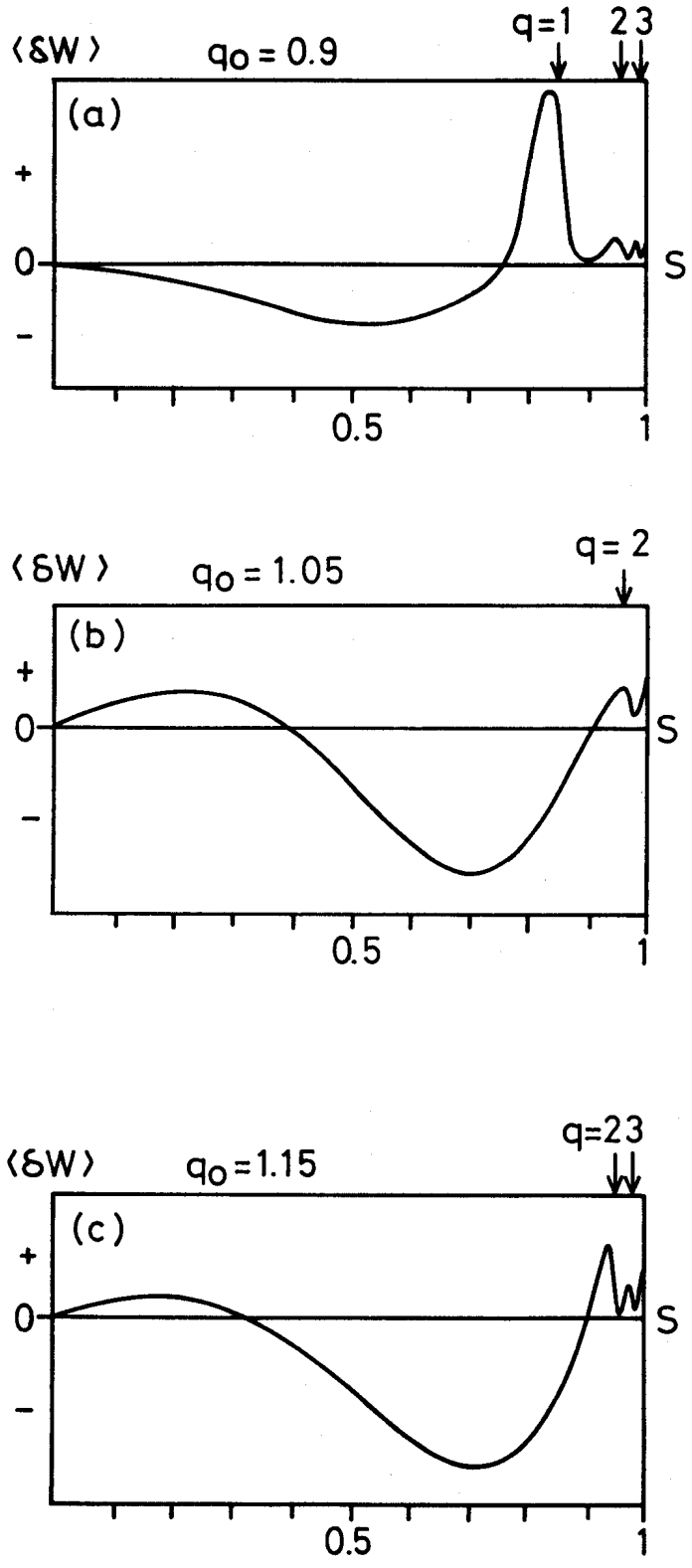

FIG. 5

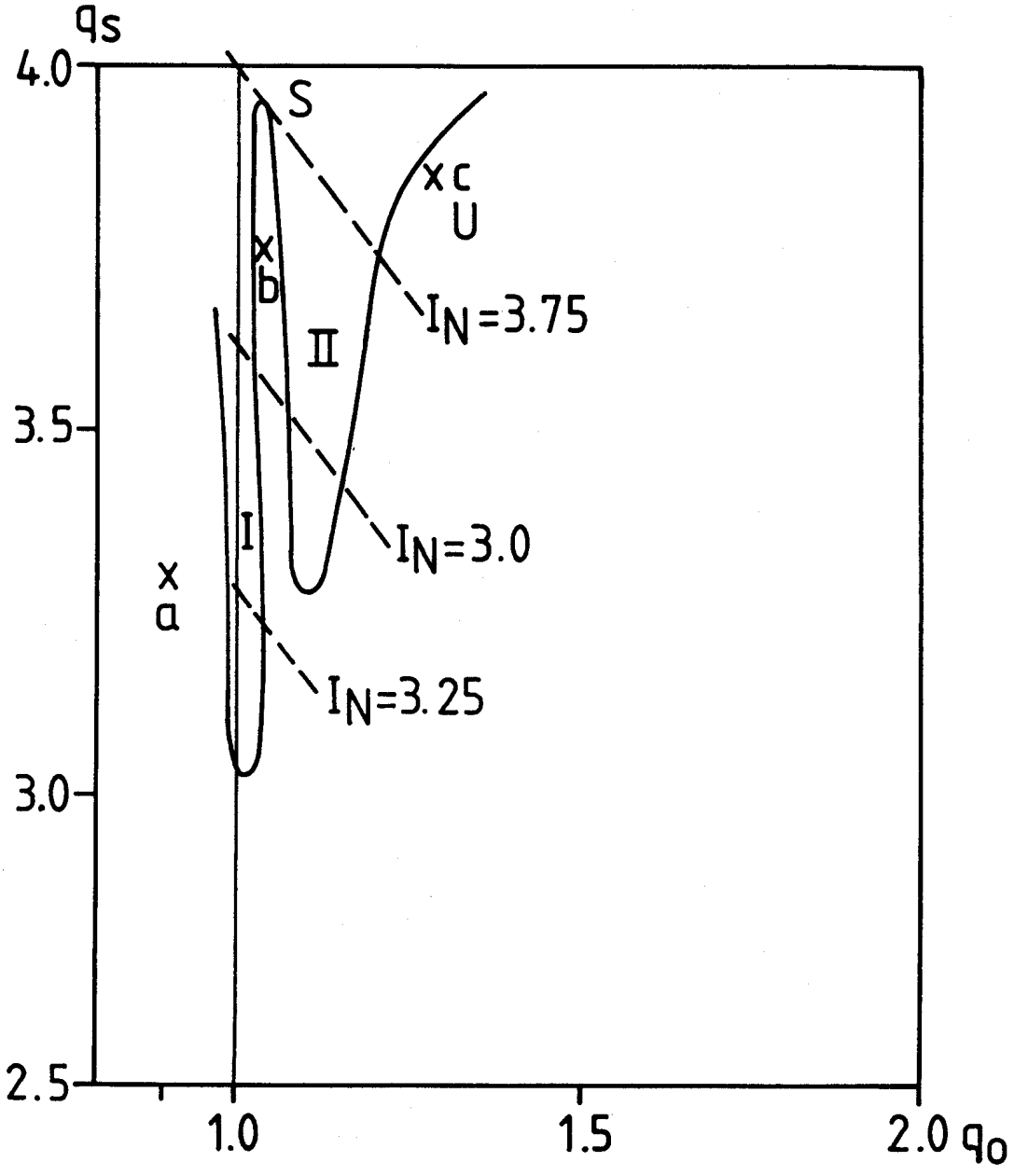

FIG. 6

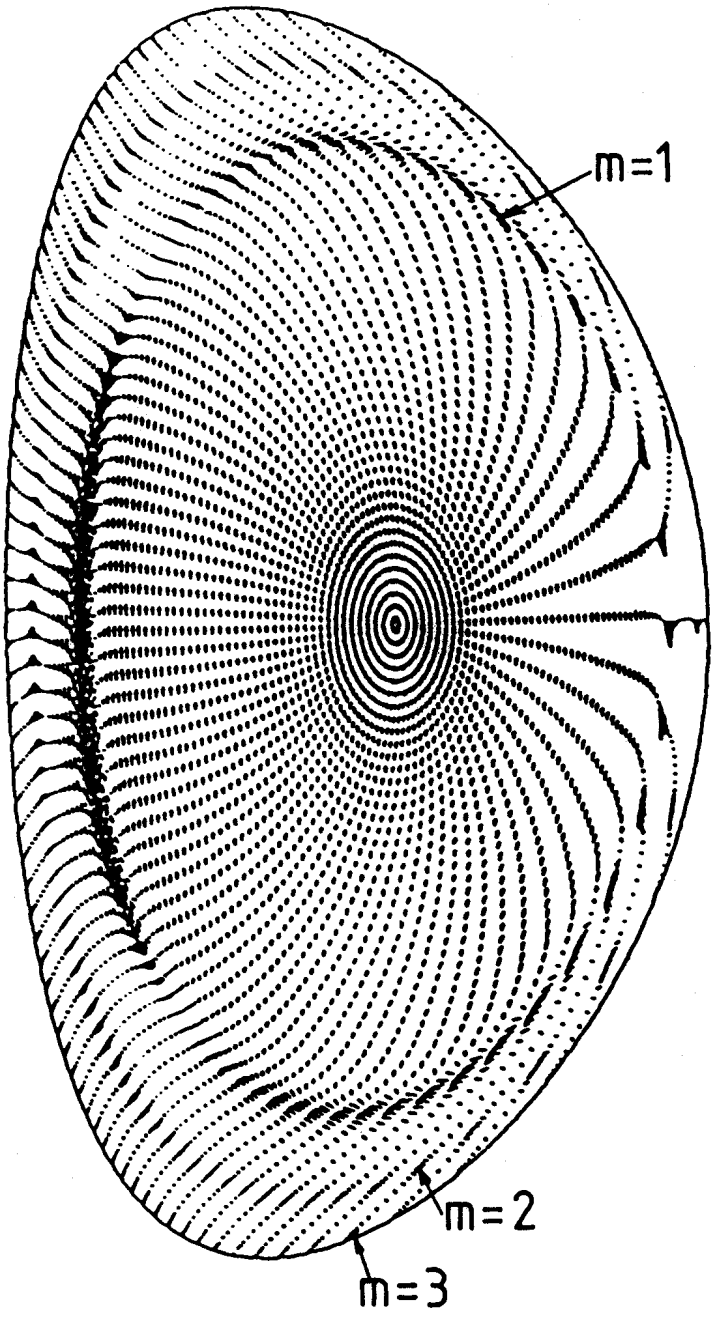

FIG. 7A

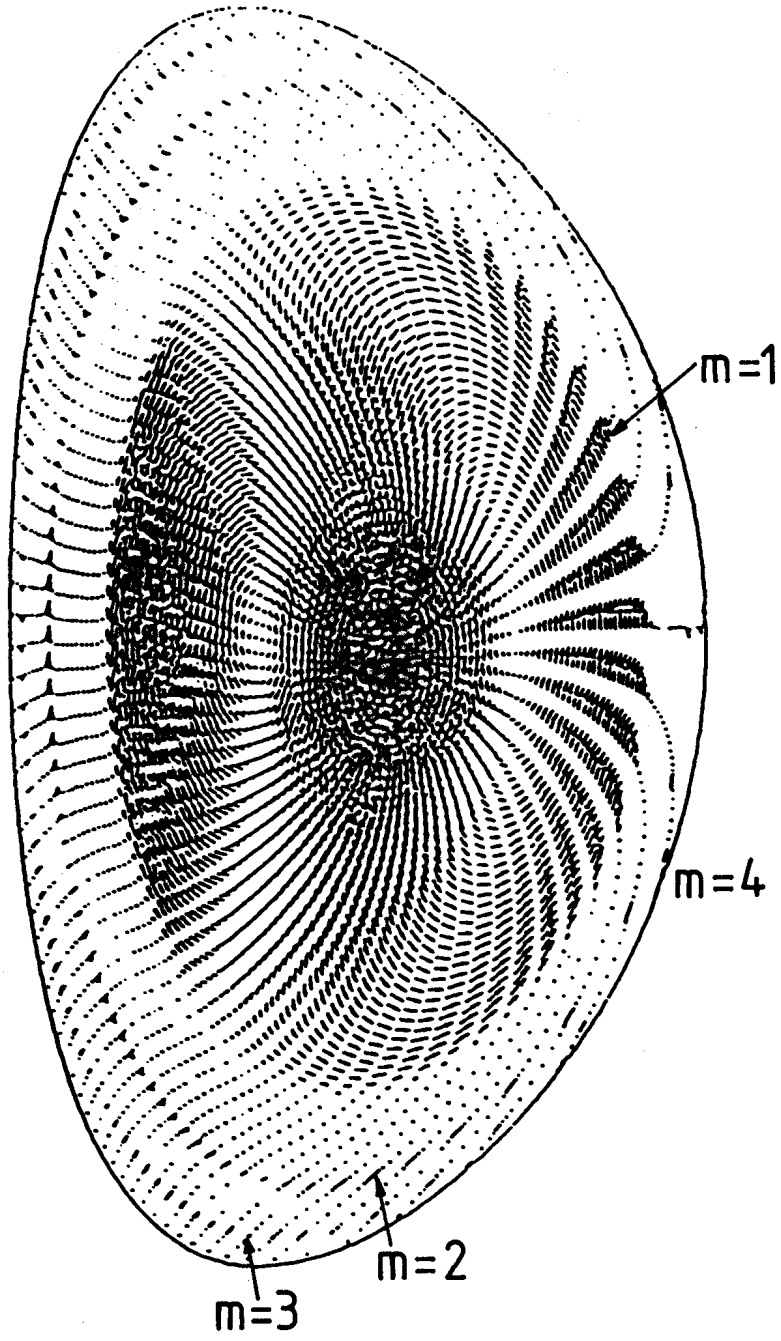

FIG. 7B

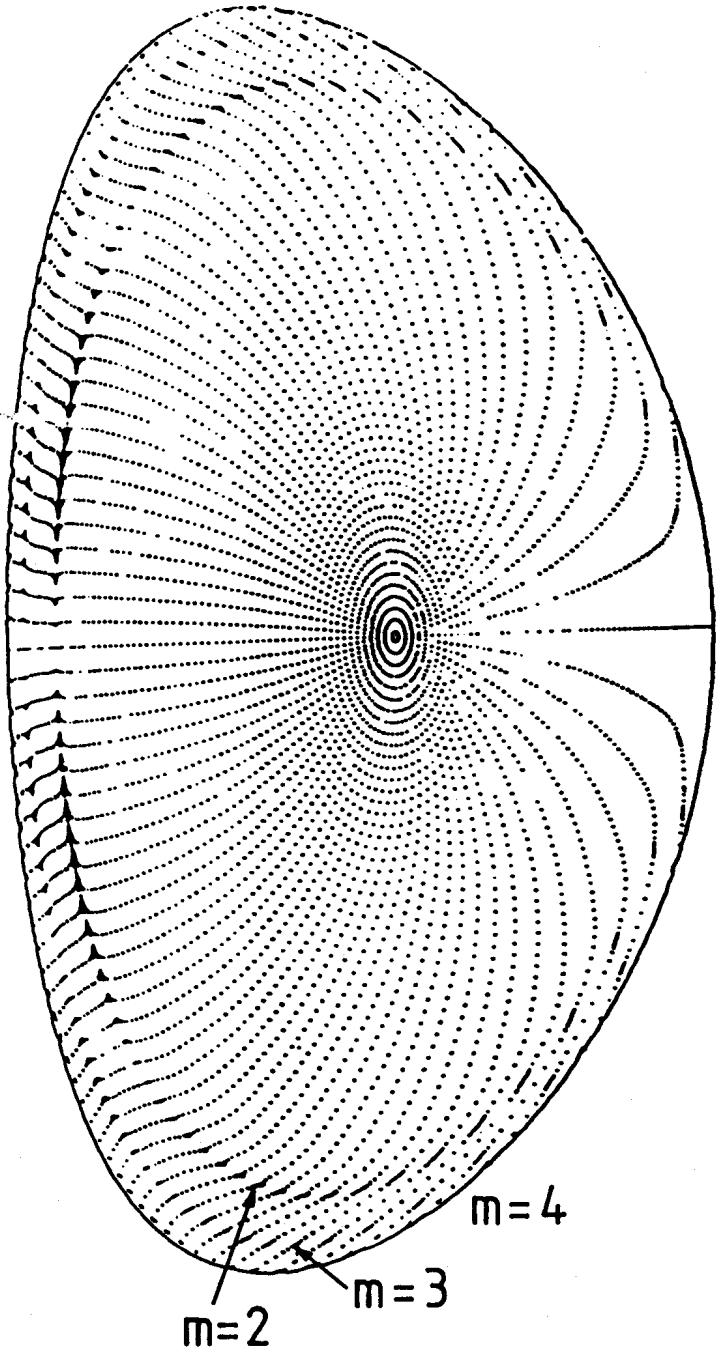

FIG. 7c

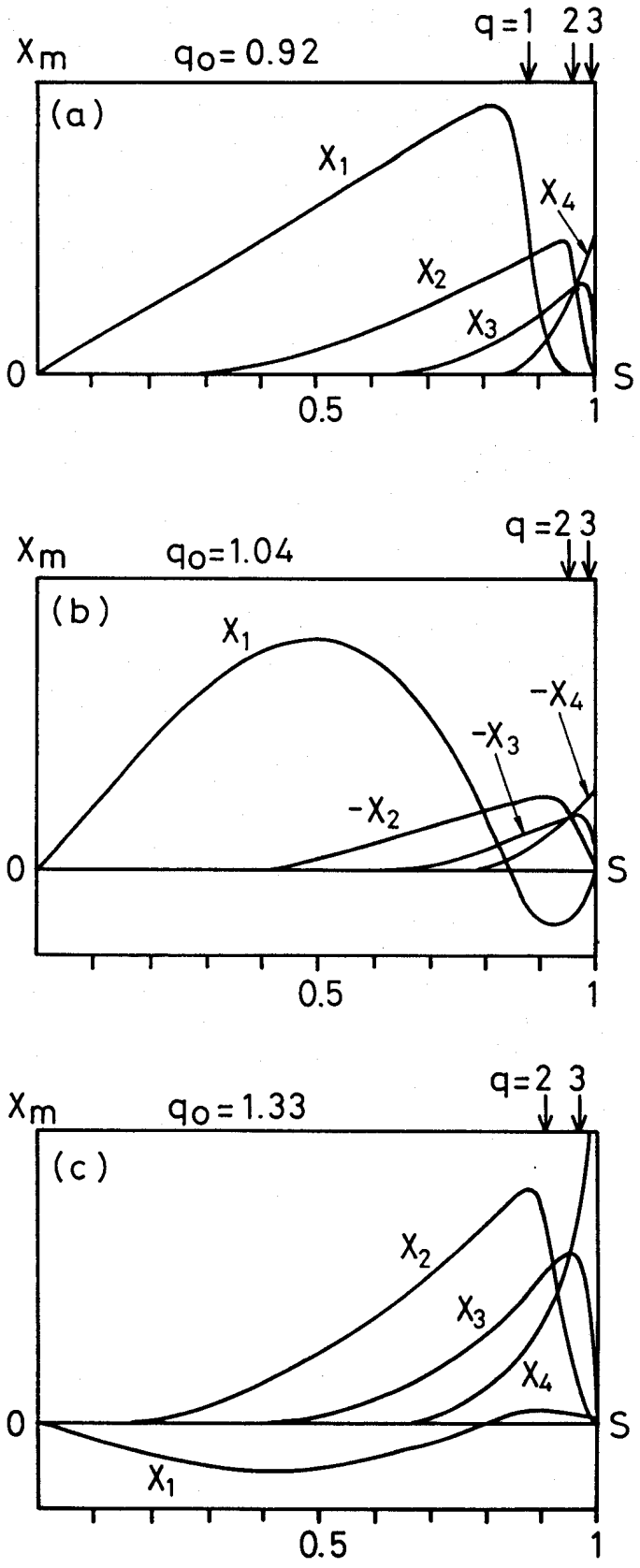
q=1 2 3
Xm
qo= 0.92
(a)
X1
X4
X2
X3
0
S
0.5
1
q=2 3
Xm
qo=1.04
(b)
X1
-X4
-X3
-X2
0
S
0.5
1
q=2 3
Xm
qo=1.33
(c)
X2
X3
X4
0
S
X1
0.5
1

FIG. 8

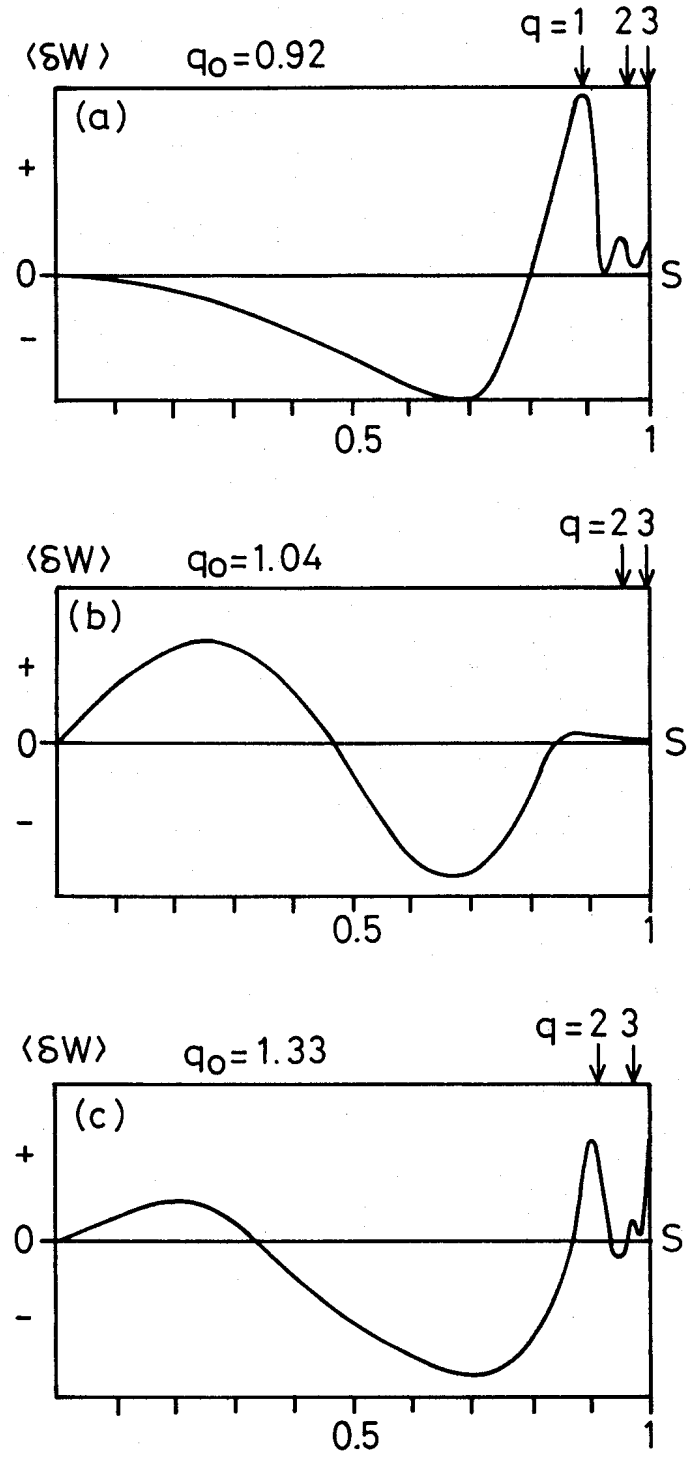

FIG. 9